Research Square

Preprints are preliminary reports that have not undergone peer review.
They should not be considered conclusive, used to inform clinical practice,
or referenced by the media as validated information.

Preoperative Prediction of Tumor Deposits in Rectal Cancer Using Cellular Microstructural Parameters Derived from Time-Dependent Diffusion MRI

Siqi Yi
Sichuan Cancer Hospital
Yanwan Li
Sichuan Cancer Hospital
Ping Zheng
Sichuan Cancer Hospital
Yehan Zhou
Sichuan Cancer Hospital
Meining Chen
Siemens Healthineers Ltd.
Thorsten Feiweier
The Siemens Healthineers AG
Fan Yang
Sichuan Cancer Hospital
Peng Zhou
Sichuan Cancer Hospital
Xiaolei Dong
Sichuan Cancer Hospital
Xiaoli Chen
xiaoli.chen@ki.se

Sichuan Cancer Hospital

Research Article

Keywords: Rectal cancer, Tumor deposits, Time-dependent diffusion magnetic resonance imaging, Cellular microstructural parameters, Apparent diffusion coefficient

Posted Date: November 18th, 2026

DOI: https://doi.org/10.21203/rs.3.rs-11593487/v1

License: This work is licensed under a Creative Commons Attribution 4.0 International License.
Read Full License

Additional Declarations: No competing interests reported.

Preoperative Prediction of Tumor Deposits in Rectal Cancer Using Cellular Microstructural Parameters Derived from Time-Dependent Diffusion MRI

Abstract

Purpose: To evaluate the efficacy of time-dependent diffusion MRI (td-dMRI)-derived quantitative parameters in preoperatively predicting tumor deposits (TD) in rectal cancer.

Methods: A total of 108 patients with rectal cancer who underwent preoperative td-dMRI, classified by pathology as TD-negative (n = 86) or TD-positive (n = 22). td-dMRI-derived parameters, including cell diameter (d), intracellular volume fraction (Vin), extracellular diffusion coefficient (Dex), cellularity, and ADC-related metrics, were measured. Firth-penalized logistic regression was performed to identify predictors and construct a predictive model. Diagnostic performance was evaluated using receiver operating characteristic (ROC) curves with bootstrap internal validation. Correlations between td-dMRI-derived parameters and pathological measurements were assessed by pearson correlation analysis in a subset of 19 patients.

Results: The Pos-TD group showed a significantly higher d value than the Neg-TD group (14.35 (IQR, 13.40-15.44) vs. 13.31 (IQR, 12.63-14.21), $P = 0.041$). Logistic regression analyses showed that d and $ADC_{OGSE25Hz}$ were associated with TD positivity (all $P < 0.05$). The combined model achieved an area under the curve (AUC) of 0.791 (0.693, 0.890) and a bootstrap-corrected AUC of 0.785 (0.675, 0.886), outperforming individual parameters and mrTD (*all* $P < 0.05$). td-dMRI-derived d, Vin, and cellularity showed moderate-to-strong correlations with pathological findings ($r = 0.702$, 0.646, and 0.694, respectively).

Conclusion: The combined model incorporating d and $ADC_{OGSE25Hz}$ demonstrated preliminary potential for preoperative prediction of TD in rectal cancer.

Keywords: Rectal cancer; Tumor deposits; Time-dependent diffusion magnetic resonance imaging; Cellular microstructural parameters; Apparent diffusion coefficient

Abbreviations:

td-dMRI: time-dependent diffusion magnetic resonance imaging

ADC: apparent diffusion coefficient;

IMPULSED: imaging microstructural parameters using limited spectrally edited diffusion;

OGSE: oscillating gradient spin-Echo;

PGSE: pulsed gradient spin-Echo;

Dex: extracellular diffusion coefficient;

Vin: intracellular volume fraction.

Background

Accurate preoperative risk stratification is essential for individualized treatment of rectal cancer [1, 2]. Tumor deposits (TD) are discrete tumor nodules in perirectal or pericolic adipose tissue without identifiable lymph node architecture, vascular walls, or neural structures [3]. The presence of TD is an established adverse prognostic factor linked to higher rates of local recurrence, distant metastasis, and diminished overall survival, making preoperative identification valuable for therapeutic planning and prognostic assessment [3, 4].

The diagnosis of TD mainly relies on postoperative histopathology, while effective noninvasive preoperative prediction remains lacking [3, 5]. Conventional rectal MRI plays a pivotal role in local staging, but small, irregular TDs can resemble metastatic lymph nodes, fibrotic strands, or peritumoral vessels [6]. Although diffusion-weighted imaging (DWI) and the apparent diffusion coefficient (ADC) are widely used to evaluate tumor cellularity and aggressiveness [7, 8], conventional ADC reflects the average motion of water molecules and provide limited information about deeper tissue microstructure [9]. In contrast, time-dependent diffusion MRI (td-dMRI) combines pulsed gradient spin-echo (PGSE) and oscillating gradient spin-echo (OGSE) to probe water diffusion across different effective diffusion times [10]. The imaging microstructural parameters using limited spectrally edited diffusion (IMPULSED) estimates cell diameter (d), intracellular volume fraction (Vin), extracellular diffusion coefficient (Dex), and cellularity [11]. In addition, the relative ADC change (rcADC) reduces interindividual variability by using the ratio of ADC values obtained at different frequencies, which may inform metastatic risk assessment [12].

Previous studies reported that td-dMRI-derived cellularity outperforms conventional ADC in distinguishing benign from malignant breast lesions [13]. It serves as a biomarker for identifying molecular subtypes and assessing response to neoadjuvant chemotherapy [14] and predicting CK19-positive hepatocellular carcinoma [15]. Integrating td-dMRI metrics with maximum tumor diameter and TI-RADS category has demonstrated significant efficacy in distinguishing benign thyroid nodules from papillary thyroid carcinoma [16]. In rectal cancer, microstructural parameters have been validated for predicting histopathological differentiation and Ki-67 expression, but their utility in the risk stratification of TD remains unexplored [17]. Given that TD-positive rectal cancers usually exhibit greater biological aggressiveness and more complex microstructural alterations [18, 19], td-dMRI-derived parameters may serve as promising imaging biomarkers for the preoperative prediction of TD.

This study evaluated td-dMRI-derived microstructural and ADC metrics for preoperative TD prediction in rectal cancer. We also examined correlations with histopathological measurements to assess their biological relevance.

Methods

Patient Characteristics

This retrospective study followed the Standards for Reporting Diagnostic Accuracy Studies (STARD) and received institutional review board approval (No. 2023GJHZ0103). All participants provided written informed consent. Between December 2023 and March 2026, 123 patients with suspected rectal cancer who underwent radical resection were enrolled. Inclusion criteria: (1) radical resection with histopathologically confirmed rectal cancer; (2) high-resolution rectal MRI and td-dMRI completed within 1 week preoperatively. Exclusion criteria and the participant flowchart are shown in Figure 1.

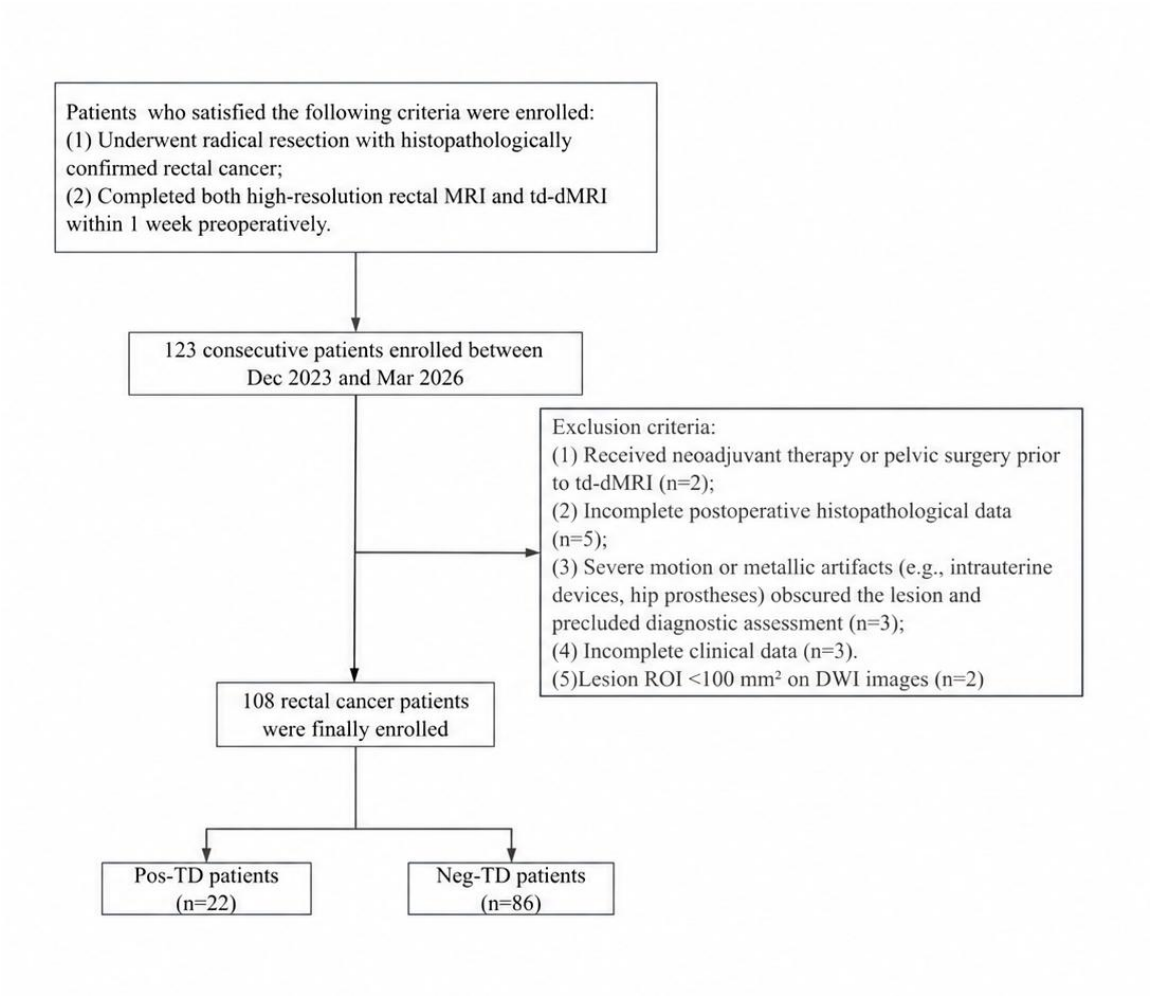


Fig. 1. Flowchart of participant enrollment

Clinical characteristics, including CEA (ng/mL), CA19-9 (U/mL), and CA242 (U/mL) were collected within 1 week before surgery, with positivity defined as CEA ≥5 ng/mL, CA19-9 ≥37 U/mL, and CA242 ≥20 U/mL.

MRI Data Acquisition

MRI was performed on a 3T MAGNETOM Skyra system (Siemens Healthineers, Forchheim, Germany) with a 32-channel body array coil and spine coil. Maximum gradient strength and slew rate were 60 mT/m and 200 mT/m/ms, respectively. A 20 ml glycerol enema was administered before scanning to reduce intestinal artifacts.

A previously described rectal cancer imaging protocol was used, including PGSE, OGSE and routine structural MRI acquisitions [17, 20]. OGSE data were acquired using a trapezoid-cosine gradient spin-echo sequence at 25 Hz (effective diffusion time = 7.1 ms; b = 0, 350, 710 s/mm²) and 40 Hz (effective diffusion time = 4.6 ms; b = 0, 150, 315 s/mm²). PGSE data were acquired with an effective diffusion time of 43.4 ms, and

b values of 0, 350, and 710 s/mm². Diffusion data were acquired along three orthogonal diffusion-encoding directions using a research single-shot echo-planar sequence. Total td-dMRI acquisition time was 4.5 minutes. OGSE, PGSE, and small-field-of-view T2WI acquisitions were prescribed perpendicular to the lesion's long axis, with identical spatial coverage and slice positioning. Acquisition details are provided in Table S1.

Image Analysis

The td-dMRI data were fitted to the IMPULSED model using the MATLAB least-squares curve fitting toolbox (MathWorks, Natick, MA, USA) to derive d, Vin, Dex, and cellularity. To improve fitting stability, fitting constraints were: $0 < d < 30$ μm, $0 < Vin < 1$, and $0 < Dex < 3$ μm²/ms [21]. ADC_{PGSE}, $ADC_{OGSE25Hz}$, and $ADC_{OGSE40Hz}$ were calculated by log-linear fitting: $s/s_0=e^{-bD}$ [22], where S and S_0 represents signals intensity acquired with and without diffusion weighting, b represents the diffusion-weighting factor, D denotes the ADC.

Regions of interest (ROIs) were manually delineated on PGSE-DWI images using ITK-SNAP 3.2 (University of Pennsylvania, USA), with reference to small-field-of-view T2WI for lesion localization. ROIs were manually delineated on the largest solid tumor cross-section and the two adjacent slices. ROIs included as much solid tumor component as possible while avoiding necrosis, hemorrhage, cystic degeneration, and adjacent non-neoplastic tissues. Each quantitative parameter was averaged arithmetically across these three consecutive slices. The $rcADC_{OGSE25Hz}$ and $rcADC_{OGSE40Hz}$ were calculated using the following formula [23]: $rcADC_{OGSE}=[(ADC_{OGSE}-ADC_{PGSE})/ADC_{PGSE}]$

Reproducibility of td-dMRI-derived Quantitative Parameters

Two radiologists (D.X. and F.Y.), blinded to surgical and pathological findings, independently measured all quantitative parameters for inter-observer reproducibility. A senior radiologist (X.C., with more than 10 years of experience) adjudicated discrepancies exceeding 10%. D.X. repeated measurements after 1 month to assess intra-observer reproducibility.

Histopathologic Analysis

Two pathologists (Z.P. and Z.Y.) assessed TD status using the 8th AJCC TNM criteria [19,20]. Pathological TDs were defined as discrete tumor nodules within the regional lymphatic drainage territory, separate from the primary tumor. They lacked residual lymph node tissue and identifiable vascular or neural structures. Lesions with identifiable vessel walls or remnants were classified as vascular invasion, and those involving identifiable neural structures as perineural invasion.

Given the labor-intensive nature of digital pathological segmentation and quantitative microstructural measurements, histopathologic correlation analysis was performed in a subset of 19 patients (3 TD-positive and 16 TD-negative cases).

High-resolution hematoxylin and eosin (H&E)-stained sections of rectal cancer tissue were obtained from all patients at ×400 magnification by a pathologist blinded to the MRI results. The specific workflow was as follows[24]: digital slides were processed using QuPath 0.5.X (University of Edinburgh, UK) and OpenSlide (Carnegie Mellon University, USA); AI-assisted ROI annotation and automated cell detection provided measurements of cell size, count [14]. The nucleus volume-weighted diameter (d_{nuclei}) was calculated as $d_{nuclei}=\sum_n d_n^4/\sum_n d_n^3$, where n denotes cell number and d denotes diameter. Pathological d was obtained by multiplying d_{nuclei} by a scaling factor of 1.8 [14]. Pathological Vin was calculated as $Vin_{pathological}=\sum_n A_{nuclei}/A_{tissue}$, where A_{tissue} and A_{nuclei} denote total tissue area and nuclear area, respectively. Pathological cellularity was calculated from the resulting Vin and d values as $cellularity_{pathological}=(Vin_{pathological}/d_{pathological})\times 100$.

Binary Assessment of TD on Conventional MRI

Two radiologists (S.Y. and Y.L.) independently assessed mrTD on high-resolution T2WI. The criteria included an irregular mesorectal nodule separate from the primary tumor, located within or along a vein and interrupting its course, with an emerging low-signal vessel [3, 22]. A tapering “comet-tail” appearance supported mrTD with overlapping discontinuous extramural venous invasion (EMVI); continuous EMVI alone did not qualify. Patients with at least one qualifying lesion were classified as mrTD-positive. Disagreements were adjudicated by a senior radiologist (P.Z.). Initial

independent ratings determined interobserver agreement, and adjudicated classifications were used for diagnostic performance analyses. mrTD was evaluated as a patient-level imaging predictor of pathological TD positivity.

Statistical Analysis

Statistical analyses used MedCalc 22.009 (Ostend, Belgium). Categorical variables were presented as percentages (%) and compared using the χ^2 test or Fisher's exact test. Normally distributed continuous variables with homogeneous variance were expressed as mean ± SD and compared using the independent-samples *t* test. Non-normally distributed or heteroscedastic variables were expressed as median (interquartile range, IQR) and compared using Mann-Whitney U test. Bonferroni correction was applied for comparisons across the nine imaging parameters.

Intraclass correlation coefficients (ICCs) assessed quantitative measurement reproducibility, and Cohen's kappa assessed mrTD agreement; Values >0.75 indicated good agreement. Firth-penalized logistic regression was used to reduce small-sample bias. Variables with *P* value < 0.05 entered into multivariable analysis, with variance inflation factors (VIFs) assessing multicollinearity. Backward selection retained variables with P < 0.05 in the final model.

Diagnostic performance was assessed using receiver operating characteristic (ROC) curves, with AUCs compared using the DeLong test. Internal validation used 1000 unstratified patient bootstrap resamples to estimate the optimism-corrected AUC. Each resample repeated screening of all 18 candidates, backward selection and Firth fitting. Calibration was assessed using the calibration slope and Brier score. Decision curve analysis (DCA) evaluated potential clinical net benefit across threshold probabilities. Pearson coefficients assessed correlations between td-dMRI-derived and pathological microstructural parameters. A two-sided *P* value < 0.05 was considered statistically significant.

Results

Patient Characteristics

A toal of 108 patients were classified into 86 Neg-TD and 22 Pos-TD based on the presence or absence of TD on pathological reports, with 57 males (aged 66.35 ± 9.31

years) and 51 females (aged 62.73 ± 11.23 years).

Preoperative CEA differed between groups (P = 0.009), whereas other baseline characteristics did not (*all* P > 0.05; Table 1).

Table 1. Baseline Characteristics of Participants

Characteristics	Pos-TD (n=22)	Neg-TD (n=86)	Statistic	*P* value
Age (years, median [IQR])	69 (61.75, 73)	65 (58, 71)	$Z = -1.547$	0.122
Sex [n (%)]			$\chi^2 = 2.630$	0.105
Male	15 (68.18)	42 (48.84)		
Female	7 (31.82)	44 (51.16)		
Preoperative CEA [n (%)]			$\chi^2 = 6.909$	0.009*
Negative	12 (54.55)	70 (81.40)		
Positive	10 (45.45)	16 (18.60)		
Preoperative CA19-9 [n (%)]			—	0.066
Negative	17 (77.27)	79 (91.86)		
Positive	5 (22.73)	7 (8.14)		
Preoperative CA242 [n (%)]			—	0.109
Negative	16 (72.73)	75 (87.21)		
Positive	6 (27.27)	11 (12.79)		
mrT-stage			$\chi^2 = 1.405$	0.236
T1-2	3 (13.64)	22 (25.58)		
T3-4	19 (86.36)	64 (74.42)		
EMVI			$\chi^2 = 1.167$	0.280
Negative	15 (68.18)	68 (79.07)		
Positive	7 (31.82)	18 (20.93)		

Table 1. Baseline Characteristics of Participants

MRF			—	0.763
Negative	17 (77.27)	70 (81.40)		
Positive	5 (22.73)	16 (18.60)		
Location of tumor[#] [n (%)]			$\chi^2 = 0.327$	0.849
Low	8 (36.36)	28 (32.56)		
Middle	11 (50.00)	42 (48.84)		
High	3 (13.64)	16 (18.60)		
mrTD			—	0.063
Negative	15 (68.18)	74 (86.05)		
Positive	7 (31.82)	12 (13.95)		

Note: Values are presented as median (IQR) or n (%). Age was compared using the Mann–Whitney U test. Pos-TD, tumor deposit-positive; Neg-TD, tumor deposit-negative; CEA, carcinoembryonic antigen; CA19-9, carbohydrate antigen 19-9; CA242, carbohydrate antigen 242; mrT-stage, MR-assessed T stage; EMVI, extramural vascular invasion; MRF, mesorectal fascia; [#]Tumor location was classified according to the distance from the inferior tumor margin to the anal verge: low (< 5 cm), middle (5–10 cm), and high (> 10 cm); mrTD, binary assessment of TD on conventional MRI. *P < 0.05 indicates statistical significance. "—" indicates that no test statistic was reported for Fisher's exact or Fisher–Freeman–Halton exact tests.

Reproducibility Analysis

The td-dMRI-derived quantitative parameters showed good inter-observer reproducibility (*ICC*, 0.827–0.913) and intra-observer reproducibility (*ICC*, 0.842–0.932; Table S2).

Comparison of Microstructural Parameters and ADC Values across Pos-TD and Neg-TD Groups

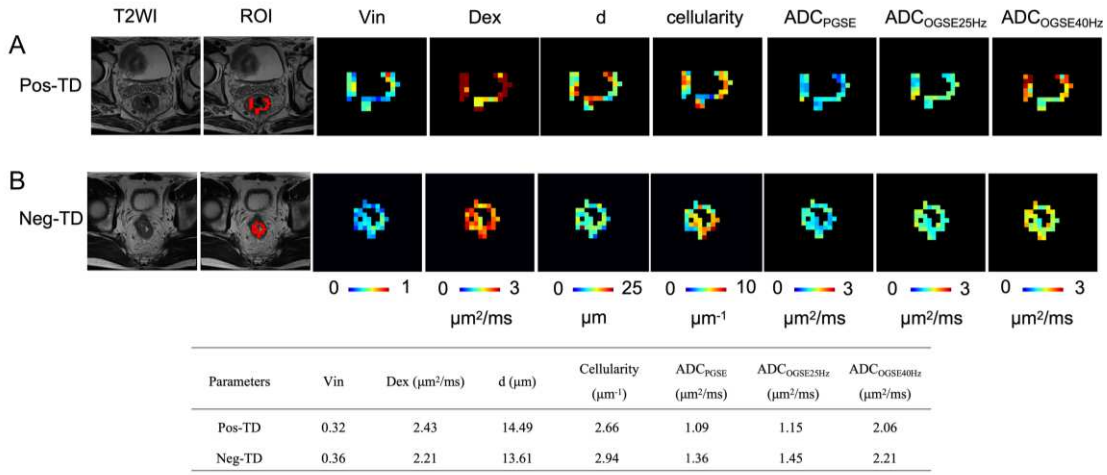
Only d was higher in the Pos-TD group than in the Neg-TD group after Bonferroni correction (median, 14.35 [IQR, 13.40-15.44] vs. 13.31 [IQR, 12.63-14.21], $P = 0.041$).

There were no significant differences observed in Vin, Dex, cellularity, ADC, and rcADC metrics after correction (all $P > 0.05$; Table 2, Figs. 2 and 3).

Table 2. Comparison of microstructural parameters derived from td-dMRI between Pos-TD and Neg-TD groups

Parameters	Pos-TD	Neg-TD	*Z/t* Value	Raw *P* value	Corrected *P* value
Vin	0.32 (0.28, 0.38)	0.33 (0.25, 0.38)	0.309	0.757	1.000
Dex ($\mu m^2/ms$)	2.50 ± 0.31	2.51 ± 0.31	−0.094	0.926	1.000
d (μm)	14.35 (13.40, 15.44)	13.31(12.63, 14.21)	2.834	0.005	0.041*
Cellularity (μm^{-1})	2.43 ± 0.66	2.75 ± 0.84	−1.893	0.066	0.590
ADC_{PGSE} ($\mu m^2/ms$)	1.14 (1.05, 1.25)	1.26 (1.12, 1.46)	−2.563	0.010	0.093
$ADC_{OGSE25Hz}$ ($\mu m^2/ms$)	1.43 (1.29, 1.50)	1.49(1.37, 1.66)	−2.052	0.040	0.362
$ADC_{OGSE40Hz}$ ($\mu m^2/ms$)	1.79 (1.70, 2.01)	1.86 (1.69, 2.14)	−0.919	0.358	1.000
$rcADC_{OGSE25Hz}$	0.18 (0.15, 0.28)	0.18(0.11, 0.24)	1.224	0.221	1.000
$rcADC_{OGSE40Hz}$	0.63 (0.45, 0.82)	0.48 (0.34, 0.64)	2.185	0.029	0.260

Note: Pos-TD, tumor deposits positive; Neg-TD, tumor deposits negative; Vin, intracellular volume fraction; Dex, extracellular diffusion coefficient; d, cell diameter; ADC_{PGSE}, apparent diffusion coefficient (ADC) measurement at pulsed gradient spin echo (PGSE); $ADC_{OGSE25Hz}$, ADC measurement at oscillating gradient spin-echo (OGSE) 25 Hz; $ADC_{OGSE40Hz}$, ADC measurement at OGSE 40 Hz; $rcADC_{OGSE25Hz}$, relative ADC measurement at OGSE 25 Hz; $rcADC_{OGSE40Hz}$, relative ADC measurement at OGSE 40 Hz. *$P < 0.05$ indicates statistical significance. Vin and rcADC values are presented on the original unscaled ratio scale.



Parameters	Vin	Dex (μm²/ms)	d (μm)	Cellularity (μm⁻¹)	ADC_{PGSE} (μm²/ms)	$ADC_{OGSE25Hz}$ (μm²/ms)	$ADC_{OGSE40Hz}$ (μm²/ms)
Pos-TD	0.32	2.43	14.49	2.66	1.09	1.15	2.06
Neg-TD	0.36	2.21	13.61	2.94	1.36	1.45	2.21

Fig. 2. The pictures are T2WI map, the region of interest (ROI), intracellular volume fraction (Vin), extracellular diffusion coefficient (Dex), cell diameter (d), cellularity, apparent diffusion coefficient (ADC) measurement at pulsed gradient spin echo (PGSE) (ADC_{PGSE}), ADC measurement at oscillating gradient spin-echo (OGSE) 25 Hz ($ADC_{OGSE25Hz}$), ADC measurement at OGSE 40 Hz ($ADC_{OGSE40Hz}$). (A) Images in a 71-year-old male patient with rectal adenocarcinoma with tumor deposits (TD). (B) Images in a 57-year-old male patient with rectal adenocarcinoma without TD.

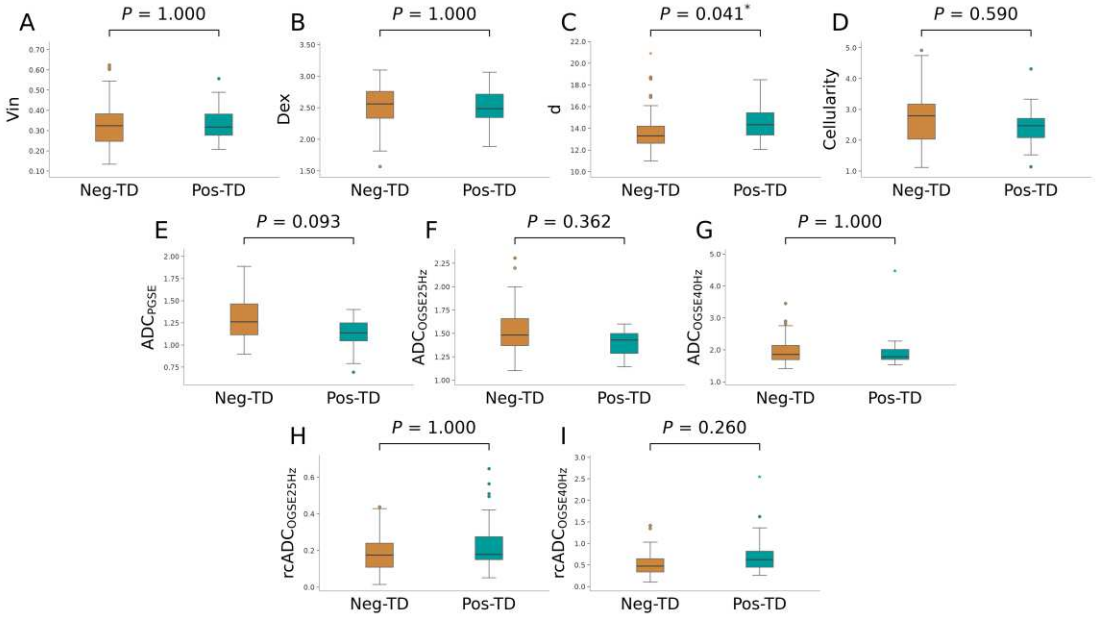


Fig. 3. Box-and-whisker plots showed distribution of the microstructural parameters and apparent diffusion coefficient (ADC) values. Dots represent individual data points, stars represent extreme outliers, and lines indicate means ± SDs. * $P < 0.05$ (A) Vin, intracellular volume fraction. (B) Dex, extracellular diffusion coefficient. (C) d, cell diameter. (D) cellularity. (E) ADC_{PGSE}, ADC measurement at pulsed gradient spin echo (PGSE). (F) $ADC_{OGSE25Hz}$, ADC measurement at oscillating gradient spin-echo (OGSE) 25 Hz. (G) $ADC_{OGSE40Hz}$, ADC measurement at OGSE 40 Hz. (H) $rcADC_{OGSE25Hz}$, relative ADC measurement at OGSE 25 Hz. (I) $rcADC_{OGSE40Hz}$, relative ADC measurement at OGSE 40 Hz. *P* values were corrected by Bonferroni.

Model Construction

CEA, d, ADC_{PGSE}, $ADC_{OGSE25Hz}$, $rcADC_{OGSE25Hz}$_per0.1and $rcADC_{OGSE40Hz}$_per0.1 were associated with TD positivity in univariable analysis(all $P < 0.05$) and entered multivariable analysis. The final model retained d (OR = 1.588, $P = 0.001$) and $ADC_{OGSE25Hz}$ (OR = 0.016, $P = 0.001$; Table 3).

Table 3. Firth-penalized logistic regression analysis for clinical characteristics, conventional MRI assessments, and microstructural parameters for predicting TD in rectal cancer.

Parameters	Univariable analysis		Multivariable analysis	
	Odds Ratio (95% CI)	*P value*	Odds Ratio (95% CI)	*P value*
Clinical characteristics				
Age	1.040 (0.992, 1.098)	0.110		
Sex				
Male	Reference			
Female	0.462 (0.167, 1.186)	0.110		
Preoperative CEA				
Negative	Reference			
Positive	3.589 (1.338, 9.657)	0.012*		
Preoperative CA19-9				
Negative	Reference			
Positive	3.331 (0.945, 11.243)	0.061		
Preoperative CA242				
Negative	Reference			
Positive	2.586 (0.826, 7.672)	0.100		
Conventional MRI assessments				
mrT-stage				
T1-2	Reference			
T3-4	1.944 (0.622, 7.876)	0.267		
EMVI				
Negative	Reference			

Table 3. Firth-penalized logistic regression analysis for clinical characteristics, conventional MRI assessments, and microstructural parameters for predicting TD in rectal cancer.

Positive	1.792 (0.627, 4.851)	0.267		
MRF				
Negative	Reference			
Positive	1.343 (0.416, 3.875)	0.604		
Location of tumor[#]		0.887		
Low	Reference			
Middle	0.907 (0.333, 2.542)	0.850		
High	0.711 (0.157, 2.692)	0.625		
td-dMRI microstructural parameters				
Vin_per0.1	1.064 (0.666, 1.660)	0.790		
Dex ($\mu m^2/ms$)	0.908 (0.205, 4.274)	0.900		
d (μm)	1.358 (1.061, 1.780)	0.015*	1.588 (1.199, 2.195)	0.001*
Cellularity (μm^{-1})	0.607 (0.312, 1.107)	0.106		
ADC_{PGSE} ($\mu m^2/ms$)	0.035 (0.002, 0.336)	0.003*		
$ADC_{OGSE25Hz}$ ($\mu m^2/ms$)	0.052 (0.003, 0.579)	0.014*	0.016 (<0.001, 0.225)	0.001*
$ADC_{OGSE40Hz}$ ($\mu m^2/ms$)	1.120 (0.322, 2.930)	0.831		
$rcADC_{OGSE25Hz}$_per0.1	1.547 (1.076, 2.278)	0.019*		
$rcADC_{OGSE40Hz}$_per0.1	1.190 (1.046, 1.397)	0.007*		

Note:TD, tumor deposit; CI, confidence interval; CEA, carcinoembryonic antigen; CA19-9, carbohydrate antigen 19-9; CA242, carbohydrate antigen 242; mrT-stage, MR-assessed T stage; EMVI, extramural vascular invasion; MRF: mesorectal fascia; [#]Tumor location was classified according to the distance from the inferior tumor margin to the anal verge: low (< 5 cm), middle (5-10 cm), and high (> 10 cm); td-dMRI, time-dependent diffusion MRI; Vin, intracellular volume fraction; Dex, extracellular diffusion coefficient; d, cell diameter; ADC_{PGSE}, apparent diffusion coefficient (ADC) measurement at pulsed gradient spin echo (PGSE); $ADC_{OGSE25Hz}$, ADC measurement at oscillating gradient spin-echo (OGSE) 25 Hz; $ADC_{OGSE40Hz}$, ADC measurement at OGSE 40 Hz; $rcADC_{OGSE25Hz}$, relative ADC measurement at OGSE 25 Hz;

Table 3. Firth-penalized logistic regression analysis for clinical characteristics, conventional MRI assessments, and microstructural parameters for predicting TD in rectal cancer.

rcADC$_{OGSE40Hz}$, relative ADC measurement at OGSE 40 Hz. * $P < 0.05$ indicates statistical significance. ORs for Vin and rcADC are per 0.1 increase in the original dimensionless ratio (analysis variable = 10 × original ratio).

The VIF values were 1.075 for both d and ADC$_{OGSE25Hz}$, indicating no substantial multicollinearity in the final model. The combined model score was $score$=-1.780+0.462×d-4.134×$ADC_{OGSE25Hz}$, and TD positivity was obtained using the logistic transformation: $P = 1/(1+e^{-Combined\ model\ score})$.

Diagnostic Performanceof Parameters and Risk Model

The combined model achieved an AUC of 0.791 (0.693, 0.890), exceeding d (AUC = 0.697, P = 0.026), ADC$_{OGSE25Hz}$ (AUC = 0.642, P = 0.014), and mrTD (AUC = 0.589, P = 0.008) on DeLong tests (Table 4, Fig. 4). The bootstrap-corrected AUC was 0.785 (0.675, 0.886), the apparent calibration slope was 1.071, and the Brier score was 0.138.

Table 4. Diagnostic performance of td-dMRI derived microstructural parameters, the combined-model, and mrTD for predicting TD in rectal cancer.

Parameters	AUC (95% CI)	Accuracy (95% CI)	Sensitivity (95% CI)	Specificity (95% CI)	Cut-off (95% CI)
d (μm)	0.697 (0.572, 0.821)	0.694 (0.500, 0.843)	0.682 (0.409, 0.955)	0.698 (0.407, 0.919)	> 13.836 (13.086, 15.095)
ADC$_{OGSE25Hz}$	0.642 (0.528, 0.757)	0.500 (0.407, 0.769)	0.955 (0.545, 1.000)	0.384 (0.256, 0.814)	< 1.543 (1.331, 1.622)
Combined-model	0.791 (0.693, 0.890)	0.713 (0.583, 0.780)	0.818 (0.545, 1.000)	0.686 (0.488, 0.919)	> 0.191 (0.125, 0.335)
Optimism-corrected performance	0.785 (0.675, 0.886)	0.688 (0.512, 0.855)	0.762 (0.509, 0.944)	0.669 (0.423, 0.921)	—
mrTD	0.589 (0.483, 0.696)	0.750 (0.676, 0.824)	0.318 (0.136, 0.545)	0.860 (0.779, 0.930)	Positive

Note: td-dMRI, time-dependent diffusion magnetic resonance imaging; TD, tumor deposit; ADC, apparent diffusion coefficient; d, cell diameter; ADC$_{OGSE25Hz}$, ADC measurement at oscillating gradient spin-echo (OGSE) 25 Hz; Combined-model, combining d and ADC$_{OGSE25Hz}$; mrTD, binary assessment of TD on

Table 4. Diagnostic performance of td-dMRI derived microstructural parameters, the combined-model, and mrTD for predicting TD in rectal cancer.

conventional MRI. Bias-corrected values were obtained by bootstrap (B = 1000, repetition). "—" No applicable cutoff.

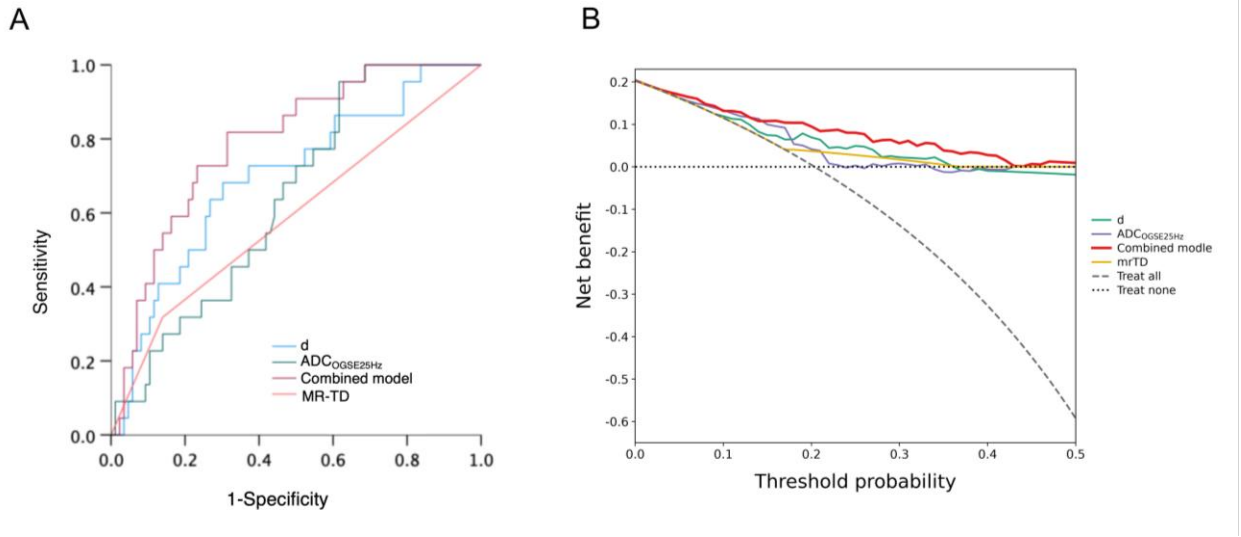


Fig. 4. (A) Receiver operating characteristic (ROC) curves of d, ADC measurement at oscillating gradient spin-echo (OGSE) 25 Hz ($ADC_{OGSE25Hz}$), the combined model for predicting TD, and mrTD. (B) Decision curve analysis (DCA) of d, $ADC_{OGSE25Hz}$, the combined model, and mrTD.

DCA indicated higher net benefit for the combined model than individual parameters, mrTD, and treat-all or treat-none strategies over thresholds of approximately 0.02–0.50 (Fig. 4B).

Binary assessment of TD on conventional MRI

mrTD showed good interobserver agreement (*kappa* = 0.834; 95% CI: 0.694–0.974) and with no significant difference between the two groups ($P = 0.063$; Table 1). The AUC of mrTD was 0.589 (0.483, 0.696), with an accuracy, sensitivity, and specificity of 0.750 (0.676, 0.824), 0.318 (0.136, 0.545), and 0.860 (0.779, 0.930) (Table 4 and Fig. 4).

Correlations with Histopathological Measurements

Imaging-derived d ($r = 0.702$, $P = 0.001$), Vin ($r = 0.646$, $P = 0.003$), and

cellularity (r = 0.694, P = 0.001) correlated positively with their pathological counterparts in the 19-patient subset (Fig. 5).

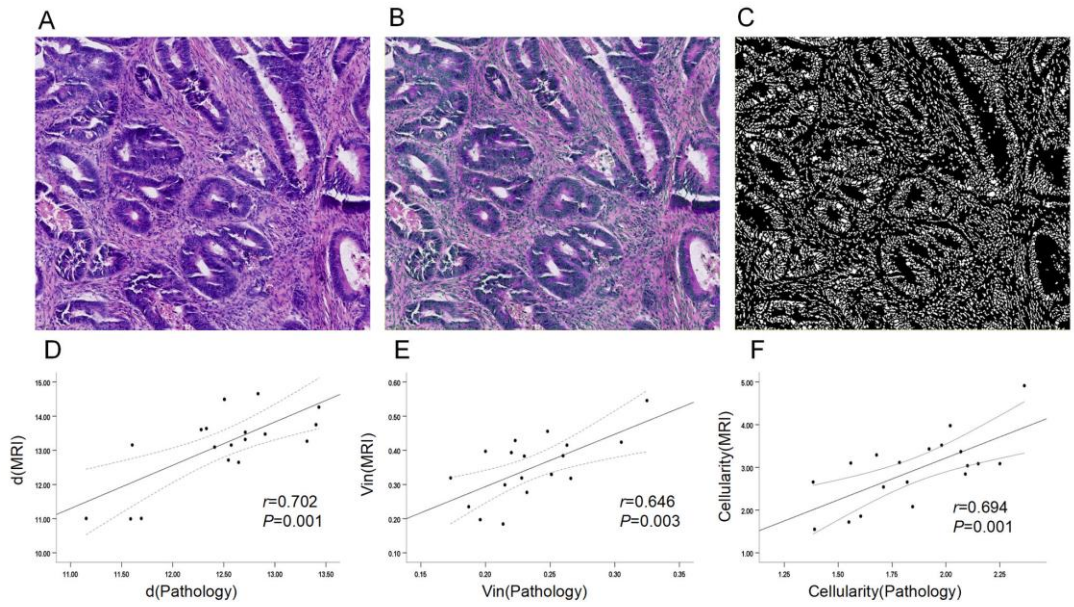


Fig. 5. Correlation analysis between td-dMRI microstructural parameters and microstructural characteristics derived by pathological examination (n = 19). (A) Hematoxylin-Eosin (H&E) staining of patients' pathological specimens (×400 magnification). (B) Nucleus visualization of HE-staining image (×400 magnification) following segmentation using a pre-trained conditional generative adversarial network. (C) Automatic quantification results of pathological microstructural measurements. (D) Correlation between MRI parameter d and pathological parameter d. (E) Correlation between MRI parameter Vin and pathological parameter Vin. (F) Correlation between MRI parameter cellularity and pathological parameter cellularity.

Discussion

In this study, we explored the potential value of td-dMRI-derived cellular microstructural parameters and ADC-related metrics for preoperative prediction of TD in rectal cancer, and examined their correspondence with histopathologic microstructural measurements. The main findings were as follows: TD-positive tumors showed a significantly larger d than TD-negative tumors after correction for multiple comparisons; d and $ADC_{OGSE25Hz}$ were retained in the Firth-penalized multivariable

regression model; the combined model achieved an AUC of 0.791 and a bootstrap-corrected AUC of 0.785; and td-dMRI-derived d, Vin, and cellularity showed moderate-to-strong correlations with pathological measurements. These findings suggest that td-dMRI may provide quantitative, biologically interpretable information for characterizing the microstructural phenotype associated with TD risk.

Preoperative identification of TD is clinically important because TD is associated with aggressive disease and adverse prognosis, but confident recognition on conventional MRI remains challenging [1, 4]. The high specificity but low sensitivity of mrTD in this cohort indicates that morphological assessment misses some pathologically positive cases. The combined td-dMRI model showed a significantly higher AUC than mrTD. Quantitative td-dMRI may therefore complement high-resolution rectal MRI, particularly when perirectal nodules are equivocal or morphological findings are discordant.

As the only parameter differing between groups after multiplicity correction, d is central to TD risk stratification. Larger d in TD-positive tumors reflects atypical cellular morphology, disordered growth, and intracellular complexity associated with aggressive behavior [5, 25]. This finding parallels the association between larger cancer cell diameter and lymph node metastasis reported in breast cancer [26]. Both lymph node metastasis and TD indicate poor prognosis. In rectal cancer patients with TD, such microstructural disorganization facilitates tumor budding, stromal infiltration, and extranodal spread—processes closely associated with TD formation [27, 28]. The strong correlation between imaging-derived and pathological d further supports the biological plausibility, although this mechanism should be confirmed in larger pathology-matched cohorts [21].

$ADC_{OGSE25Hz}$ contributed complementary predictive information. $ADC_{OGSE25Hz}$ represents the absolute ADC measured with OGSE at 25 Hz and therefore probes water diffusion at an effective diffusion time between those of PGSE and OGSE at 40 Hz. In this study, $ADC_{OGSE25Hz}$ showed modest diagnostic performance, and group differences were not significant after correction; yet it remained associated with TD positivity in the multivariable model. This pattern suggests that it may provide complementary

information on extracellular architecture, stromal remodeling, or diffusion-time-dependent heterogeneity that is not fully described by d [28, 29].

ADC_{PGSE} and both rcADC metrics were associated with TD positivity in univariable analysis but were not retained after backward selection. Both rcADC metrics make their interpretation dependent on the corresponding OGSE measurement and the shared ADC_{PGSE} denominator[29]. The exclusion of $rcADC_{OGSE25Hz}$ despite retention of $ADC_{OGSE25Hz}$ suggests that normalization to ADC_{PGSE} did not provide sufficient additional predictive information in this model. For $rcADC_{OGSE40Hz}$, TD-positive tumors exhibited numerically lower ADC_{PGSE} and higher $rcADC_{OGSE40Hz}$, whereas $ADC_{OGSE40Hz}$ was not significantly associated with TD positivity in univariable analysis. These suggest that the association of rcADC was partly driven by lower PGSE diffusivity rather than a distinct alteration in high-frequency diffusion.

CEA was associated with TD positivity in univariable analysis and differed between the two groups. However, it was not retained in the final multivariable model. Given the small number of TD-positive, The incremental value of CEA should therefore be reassessed alongside imaging in larger, externally validated models [14, 30].

Compared with mrTD, the combined td-dMRI model demonstrated a higher AUC for predicting TD positivity, suggesting that it can provide incremental value over conventional MRI-based binary assessment. The combined td-dMRI model integrates continuous quantitative information, which helps capture tumor microstructural heterogeneity that is not readily reflected by conventional morphologic MRI. The small decrease in AUC after bootstrap correction suggested limited optimism in model discrimination, while the Brier score and calibration slope supported acceptable apparent calibration [31, 32].

This study has several limitations. First, the retrospective single-center design and 22 TD-positive events may increase selection instability and overfitting, requiring external validation in larger prospective multicenter cohorts. Second, IMPULSED assumes spherical cells, which may inadequately represent complex tumor geometry; more flexible biophysical models could improve characterization [33, 34]. Third, the three-slice ROI strategy reduced the risk of including necrosis, peritumoral fat, and

partial-volume artifacts, but it may not fully capture whole-tumor heterogeneity. Volumetric segmentation and heterogeneity features warrant investigation [35]. Fourth, exact MRI-pathology spatial matching was limited by specimen orientation differences and tissue deformation during fixation and sectioning [36].

In conclusion, the combined d and $ADC_{OGSE25Hz}$ model showed acceptable diagnostic performance and preliminary potential for preoperative TD prediction in rectal cancer.

References

1. Feng Y, Hu T, Gu W et al (2025) Mesorectal fascia involvement by tumor deposits or extramural vascular invasion at MRI predicts prognosis in rectal cancer. Radiology 317:e243627. https://doi.org/10.1148/radiol.243627
2. Winn RJ, McClure J (2003) The NCCN clinical practice guidelines in oncology: a primer for users. J Natl Compr Cancer Netw 1:5–13. https://doi.org/10.6004/jnccn.2003.0003
3. Lord AC, D'souza N, Shaw A et al (2022) MRI-diagnosed tumor deposits and EMVI status have superior prognostic accuracy to current clinical TNM staging in rectal cancer. Ann Surg 276:334–344. https://doi.org/10.1097/SLA.0000000000004499
4. Ueno H, Nagtegaal ID, Quirke P, Sugihara K, Ajioka Y (2023) Tumor deposits in colorectal cancer: Refining their definition in the TNM system. Ann Gastroenterol Surg 7:225–235. https://doi.org/10.1200/JCO.2016.68.9091
5. Lord A, Brown G, Abulafi M et al (2021) Histopathological diagnosis of tumour deposits in colorectal cancer: a Delphi consensus study. Histopathology 79:168–175. https://doi.org/10.1111/his.14344
6. Luo H, Gou YQ, Wang YS et al (2025) A novel pN stage prediction model for resectable rectal adenocarcinoma based on preoperative MRI features and multiregional apparent diffusion coefficients. Eur Radiol 35:5760–5770. https://doi.org/10.1007/s00330-025-11528-x
7. Nerad E, Delli Pizzi A, Lambregts DM et al (2019) The Apparent Diffusion Coefficient (ADC) is a useful biomarker in predicting metastatic colon cancer using the ADC-value of the primary tumor. PLoS One 14:e0211830. https://doi.org/10.1371/journal.pone.0211830

8. Schurink NW, Lambregts DM, Beets-Tan RG (2019) Diffusion-weighted imaging in rectal cancer: current applications and future perspectives. Br J Radiol 92:20180655. https://doi.org/10.1259/bjr.20180655

9. Li X, Li C, Hua B, Jiang L, Chen M (2025) Time-dependent diffusion MRI and kinetic heterogeneity as potential imaging biomarkers for diagnosing suspicious breast lesions with 3.0-T breast MRI. Magn Reson Imaging 117:110323. https://doi.org/10.1016/j.mri.2025.110323

10. Iima M, Kataoka M, Honda M, Le Bihan D (2024) Diffusion-weighted MRI for the assessment of molecular prognostic biomarkers in breast cancer. Korean J Radiol 25:623–633. https://doi.org/10.3348/kjr.2023.1188

11. Jiang X, Devan SP, Xie J, Gore JC, Xu J (2022) Improving MR cell size imaging by inclusion of transcytolemmal water exchange. NMR Biomed 35:e4799 .https://doi.org/10.1002/nbm.4799

12. Iima M, Yamamoto A, Kataoka M et al (2019) Time-dependent diffusion MRI to distinguish malignant from benign head and neck tumors. J Magn Reson Imaging 50:88–95. http://doi.org/10.1007/s00330-013-3002-z

13. Su Y, Qiu Y, Huang X et al (2025) Benign and malignant breast lesions: differentiation using microstructural metrics derived from time-dependent diffusion MRI. Radiol Imaging Cancer 7:e240287. https://doi.org/10.1148/rycan.240287

14. Wang X, Ba R, Huang Y et al (2024) Time-dependent diffusion MRI helps predict molecular subtypes and treatment response to neoadjuvant chemotherapy in breast cancer. Radiology 313:e240288. https://doi.org/10.1148/radiol.240288

15. Wei YC, Qin XQ, Li JS et al (2026) Time-dependent diffusion MRI combined with enhanced MRI and clinical indicators for preoperative prediction of CK19 expression status in hepatocellular carcinoma: a prospective study. Magn Reson Imaging 127:110602. https://doi.org/10.1016/j.mri.2025.110602

16. Ren H, Shi D, Huang J et al (2025) Differentiating Benign Thyroid Nodules and Papillary Thyroid Carcinoma Using Time-Dependent Diffusion MRI: A Feasibility Study. J Magn Reson Imaging 62:1649–1660. https://doi.org/10.1002/jmri.70065

17. Lu F, Li K, Wu R et al (2026) Time-dependent diffusion MRI derived microstructure parameters to predict differentiation degree and Ki-67 expression in rectal cancer. Eur J Radiol 195:112522. https://doi.org/10.1016/j.ejrad.2025.112522

18. Agger E, Jörgren F, Jöud A, Lydrup M, Buchwald P (2023) Negative prognostic impact of tumor deposits in rectal cancer: a national study cohort. Ann Surg 278:e526–e533. https://doi.org/10.1097/SLA.0000000000005755

19. Nagtegaal ID, Knijn N, Hugen N et al (2017) Tumor deposits in colorectal cancer: improving the value of modern staging—a systematic review and meta-analysis. J Clin Oncol 35:1119–1127. https://doi.org/10.1200/JCO.2016.68.9091

20. Lu F, Li Y, Wu R et al (2026) Microstructural mapping of time-dependent diffusion MRI for predicting lymphovascular invasion in rectal cancer: a proof-of-concept investigation. Insights Imaging 17:127. https://doi.org/10.1186/s13244-026-02299-0

21. Ba R, Wang X, Zhang Z et al (2023) Diffusion-time dependent diffusion MRI: effect of diffusion-time on microstructural mapping and prediction of prognostic features in breast cancer. Eur Radiol 33:6226–6237. https://doi.org/10.1007/s00330-023-09623-y

22. Nougaret S, Gormly K, Lambregts DM et al (2025) MRI of the rectum: a decade into DISTANCE, moving to DISTANCED. Radiology 314:e232838. https://doi.org/10.1148/radiol.232838

23. Reynaud O (2017) Time-dependent diffusion MRI in cancer: tissue modeling and applications. Front Phys 5:58. https://doi.org/10.3389/fphy.2017.00058

24. Wu D, Jiang K, Li H et al (2022) Time-Dependent Diffusion MRI for Quantitative Microstructural Mapping of Prostate Cancer. Radiology 303:578-587. https://doi.org/10.1148/radiol.211180

25. Wei H, Yang F, Wang S et al (2026) The value of time-dependent diffusion MRI in nasopharyngeal carcinoma: correlation with prognostic factors. Eur Radiol 36:6053–6067. https://doi.org/10.1007/s00330-026-12402-0

26. Chen S, Bai J, Guo X et al (2026) Utility of time-dependent diffusion MRI based microstructural parameters in predicting lymph node metastasis in breast cancer. Eur J Radiol 194:112515. https://doi.org/10.1016/j.ejrad.2025.112515

27. Prabhudesai A, Arif S, Finlayson CJ, Kumar D (2003) Impact of microscopic extranodal tumor deposits on the outcome of patients with rectal cancer. Dis Colon Rectum 46:1531–1537. https://doi.org/10.1007/s10350-004-6809-5

28. Yu XP, Wen L, Hou J et al (2016) Discrimination between metastatic and nonmetastatic mesorectal lymph nodes in rectal cancer using intravoxel incoherent motion diffusion-weighted magnetic resonance imaging. Acad Radiol 23:479–485. https://doi.org/10.1016/j.acra.2015.12.013

29. Kamimura K, Kamimura Y, Nakano T et al (2023) Differentiating brain metastasis from glioblastoma by time-dependent diffusion MRI. Cancer Imaging 23:75. https://doi.org/10.1186/s40644-023-00595-2

30. Ren H, Shi D, Wang X et al (2026) Time-dependent Diffusion MRI for Predicting Response to Induction Chemotherapy in Nasopharyngeal Carcinoma. Radiol Imaging Cancer 8:e250579. https://doi.org/10.1148/rycan.250579

31. Iba K, Shinozaki T, Maruo K, Noma H (2021) Re-evaluation of the comparative effectiveness of bootstrap-based optimism correction methods in the development of multivariable clinical prediction models. BMC Med Res Methodol 21:9. https://doi.org/10.1186/s12874-020-01201-w

32. Moons KG, Altman DG, Reitsma JB et al (2015) Transparent Reporting of a multivariable prediction model for Individual Prognosis or Diagnosis (TRIPOD): explanation and elaboration. Ann Intern Med 162:W1–W73. https://doi.org/10.7326/M14-0698

33. Panagiotaki E, Walker-Samuel S, Siow B et al (2014) Noninvasive quantification of solid tumor microstructure using VERDICT MRI. Cancer Res 74:1902–1912. https://doi.org/10.1158/0008-5472.CAN-13-2511

34. Reynaud O, Winters KV, Hoang DM, Wadghiri YZ, Novikov DS, Kim SG (2016) Pulsed and oscillating gradient MRI for assessment of cell size and extracellular space (POMACE) in mouse gliomas. NMR Biomed 29:1350–1363. https://doi.org/10.1002/nbm.3577

35. van Heeswijk MM, Lambregts DM, van Griethuysen JJ et al (2016) Automated and semiautomated segmentation of rectal tumor volumes on diffusion-weighted MRI: can it replace manual volumetry? Int J Radiat Oncol Biol Phys 94:824–831. https://doi.org/10.1016/j.ijrobp.2015.12.017

36. Alyami W, Kyme A, Bourne R (2022) Histological validation of MRI: A review of challenges in registration of imaging and whole-mount histopathology. J Magn Reson Imaging 55:11–22. https://doi.org/10.1093/neuonc/noad003

Supplementary Files

This is a list of supplementary files associated with this preprint. Click to download.

- ElectronicSupplementaryMaterial.docx